Halder, K.; Bengtson, G.; Filiz, V.; Abetz, V.:

Catalytically active (Pd) nanoparticles supported by electrospun PIM-1: Influence of the sorption capacity of the polymer tested in the reduction of some aromatic nitro compounds

In: Applied Catalysis A 55 (2018) 178 - 188
First published online by Elsevier: February 6, 2018

DOI: 10.1016/j.apcata.2018.02.004
https://doi.org/10.1016/j.apcata.2018.02.004

Catalytically active (Pd) nanoparticles supported by electrospun PIM-1: influence of the sorption capacity of the polymer tested in the reduction of some aromatic nitro compounds

Karabi Halder[1], Gisela Bengtson[1], Volkan Filiz[1], Volker Abetz[1,2]

[1] *Helmholtz-Zentrum Geesthacht, Institute of Polymer Research, Max-Planck-Strasse 1, 21502 Geesthacht, Germany*

[2] *University of Hamburg, Institute of Physical Chemistry, Martin-Luther-King-Platz 6, 20146 Hamburg, Germany*

Corresponding author: volker.abetz@hzg.de (V. Abetz)

Graphical Abstract

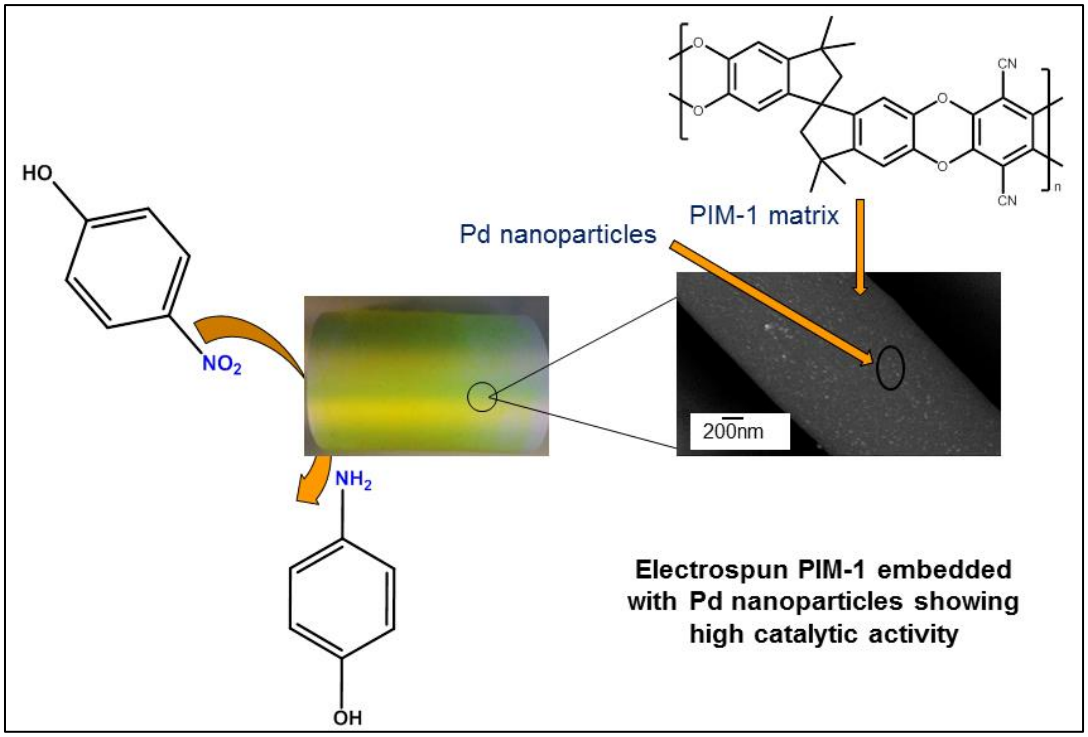

Highlights:

- The polymer of intrinsic microporosity (PIM-1) was successfully electrospun to form uniform fibers.
- For the first time PIM-1 fibers were used as support for nanoparticles (NPs) with catalytic activity.
- Catalytic reduction of *p*-nitrophenol shows almost independence of fiber diameter indicating the presence of catalytic NPs also inside the fibers.
- *p*-nitrophenol is sorbed preferentially in PIM-1 compared to larger dinitro compounds.

Abstract

Microfibers of the first so-called polymer of intrinsic microporosity (PIM-1) were prepared by electrospinning 10 wt.% PIM-1 in tetrachloroethane and used as immobilized supports for catalytic reactions. Solutions with varied concentrations of palladium diacetate ($PdAc_2$) were coated on electrospun PIM-1 to show that PIM-1 is a superior catalyst supporting material with a high surface per weight ratio. Palladium (Pd) nanoparticles (NPs) were produced via the reduction of the $PdAc_2$ with ethanol followed by subsequent thermal treatment for durably fixing of the NPs on the fibers. A comparison of the catalytic activity of PIM-1 supported PdNPs was made with that of similarly produced electrospun nanofibers of polyacrylonitrile (PAN) and polyimide (6FDA-6FpDA) with catalytic PdNPs.

The morphology of the electrospun fibers and the distribution of the Pd nanoparticles on the outer surface of the fibers were determined by scanning electron microscopy (SEM). Transmission electron microscopy (TEM) analysis of the cross section of the fibers showed the distribution of PdNPs across the fiber with a slight excess on the outer surface of the fibers. The nanoparticles (NPs) supported by the electrospun polymers catalyzed the reduction of different aromatic nitro compounds to their corresponding amino derivatives. The kinetics of the

reduction reactions were monitored by ultraviolet-visible (UV-Vis) spectroscopy. Results showed that the PdNPs supported by electrospun PIM-1 fiber possessed high activity in the reduction reaction with an only slight dependence on the fiber diameter in the case of *p*-nitrophenol, while in the case of the dinitro compounds the dependence of the kinetics on the fiber diameter was more pronounced. The catalytic tests on two dinitro compounds proved the higher sorption of PIM-1 for *p*-nitrophenol is responsible for the higher catalytic activity of PIM-1 based catalytic nanofiber mats. These results clearly show that the catalytic activity of the PIM-1 fiber mats is higher compared to the fiber mats from PAN or 6FDA-6FpDA in the case of small reactants, which is mainly due to the fact that the PdNPs are also formed within the microporous PIM-1 fibers, while this is not the case for the other more dense fibers, where the catalytic particles are located only on the outer surface.

Keywords: Polymer of intrinsic microporosity (PIM-1), electrospinning, palladium nanoparticles, catalytic activity, sorption.

1. Introduction

Noble metal nanoparticles are potential candidates in the field of nano and colloidal science due to their quantum confinement and high surface area to volume ratio. Their optical, electronic, and especially catalytic properties are directly related to the size of these zero valent metal clusters which make them more attractive than their bulk counterparts for certain applications [1]. Amongst the commonly encountered noble metals, Palladium is one of the most widely used nanomaterial based catalysts owing to its high catalytic efficiency in a wide range of chemical reactions including CO and alcohol oxidation, NO reduction, Suzuki cross coupling reaction, carbon-carbon coupling reactions, Heck's reactions and hydrogenation of olefins [2-8]. A disadvantage is certainly the price of Pd. However, a major drawback of these Pd nanoparticles (PdNPs) is their strong aggregation due to high surface energy and Van der Waals's forces which lead to the deterioration of activity and selectivity in catalytic reactions.

To suppress the formation of such agglomerates, Pd supported by activated carbon or alumina has been commonly used to produce well separated nanosized palladium particles to catalyze reactions with high reaction rate and turnover numbers [6]. However, high temperature and pressure are often the requirements of such processes. The highly inflammable H_2

(reductant) makes the process difficult to deal with. In an alternative approach to prevent particle agglomeration, Demir et al. [9] employed the electrospinning technique for directly depositing palladium nanoparticles on electrospun fibers of acrylonitrile and acrylic acid copolymers. The nanofibrous system exhibited 4.5 times higher catalytic activity than a commercial Pd/Al_2O_3 catalyst.

Electrospinning is a technique for the fabrication of thin fibers with high surface areas, under the application of a high electric field to a polymer melt or solution. This electric field generates charge on the body of the polymer jet/solution [10]. When the voltage is sufficiently high, the electrostatic repulsion on the surface of the polymer jet overcomes the surface tension of the droplet and the droplet gets stretched [11]. At a critical point, a stream of liquid erupts from the surface known as the Taylor's cone [12, 13]. As the stream of jet migrates in the air, the solvent evaporates and the charged jet left behind is deposited on the grounded collector. With a careful control of some of the parameters such as the polymer concentration, solvent, strength of the electric field, spinning distance, it is possible to obtain fibers of uniform diameter and identical morphology [14]. The high surface area to volume ratio generated by the nanosized diameter of the fibers helps in immobilizing nanoparticles or bioactive molecules, *e.g.* lipase [15] and can be attributed to their enhanced catalytic efficiency. The conventional catalyst preparation techniques are usually limited to the controlled deposition and adjusting the specific surface area of a catalyst on a support [16]. On the contrary, such catalytic nanofibers serving as immobilized supports can also control the mechanical stability, distribution, reactivity and selectivity of the catalysts.

Ebert et al. [17] used a similar electrospinning method to produce catalytically active poly(amideimide) nanofiber mats. Contrary to a previous work [9], the catalytic activation of the electrospun nanofibers has been performed by coating the fibers with a palladium diacetate solution. The coating method yields a higher catalytic activity, which has been shown by an almost seven times higher hydrogenation rate than the conventional Pd catalyst supported by alumina.

The high adsorption surface area of polymer of intrinsic microporosity (PIM-1) ($760\ m^2g^{-1}$) [18] has been explored in previous works [19, 20] with BET-measurements, to produce electrospun fibers for a variety of applications, ranging from energy storage to separation of oil-water microfiltration. One particularly interesting work involves the adsorption of contaminants from a non-aqueous system [21], where the high porosity, large surface-area to volume ratio and excellent flexibility in the PIM-1 fibers make it suitable for

organic solvent recovery having industrial relevance.

This current work is focused on exploiting the high sorption properties (for e.g. *p*-nitrophenol) and favourable inner surface area of PIM-1 for catalytic applications. The electrospun PIM-1 fibers after being coated with an organic solution of palladium diacetate (higher solubility and lesser toxicity than its corresponding chloride) have been activated by thermal treatment in air to yield well separated nanosized Pd particles on the surface of the nanofibers. The catalytic activity has been tested in the standard reduction of *p*-nitrophenol to *p*-aminophenol, in the presence of $NaBH_4$. This model reaction has been applied earlier in different systems [22, 23] to study the catalytic activity of the noble metal catalysts. In one of the studies [22] micelle supported gold (Au) nanocomposites with a polystyrene (PS) core and a poly(4-vinylpyridine) corona has been formed by the self-assembly of a PS-*b*-P4VP block copolymer in an acidic aqueous solution. The other work [23] incorporates block copolymer hollow fiber membranes of PS-*b*-P4VP with Au nanoparticles for catalytic activity. The current work relies on a relatively easy polycondensation synthesis route for PIM-1 and the nanoparticle size is solely controlled by the morphology of the PIM-1 fibers. Fibers have also been tested for three hydrogenation runs and their reproducible activity confirmed that no leaching of PdNPs occurred.

In order to establish the importance of the adsorption characteristics of PIM-1 in the catalytic reaction, a comparison has been made with a hydrophilic polyacrylonitrile (PAN) and a hydrophobic 6FDA-6FpDA polyimide supports, which were produced in the same way. The influence of sorption on the catalytic activity has been demonstrated by the use of two dinitro compounds with varying poly(ethylene glycol) (PEG) chain lengths, which cannot enter the inner part of the PIM-1 fibers.

2. Experimental Section

2.1 Materials

The monomers required for PIM-1 synthesis, 5,5',6,6'-tetrahydroxy-3,3,3',3'-tetramethyl-1,1'-spirobisindane (TTSBI, 97%) were obtained from ABCR GmbH & Co. KG (Karlsruhe, Germany) and 2,3,5,6-tetrafluoroterephthalonitrile (TFTPN, 99%) was kindly donated by Lanxess (Bitterfeld, Germany) and sublimated twice at 70°C/10^{-3} mbar prior to use. Potassium carbonate (K_2CO_3 > 99.5%) was dried at 120°C for twelve hours and then milled in a vibratory mill for ten minutes. Polyacryonitrile (PAN) (Mw 200 kDa) was purchased from Dolan (Kelheim, Germany) and was used as received. 6FDA-6FpDA polyimide (Mw 150 kDa) was synthesized according to the method as described elsewhere [24]. Ethylene glycol (99.8%) (EG)

was obtained from Acros Organics (New Jersey, USA). 1,1,2,2 tetrachloroethane (98%), 1,2-dichlorobenzene (99%) were obtained from Sigma Aldrich (Steinheim, Germany). 1-Fluoro-4-nitrobenzene (99%), poly(ethylene glycol) 2000 (PEG 2000), dimethyl formamide (DMF, 99.8%), ethyl acetate and ethanol were purchased from Merck (Darmstadt, Germany) and used as received.

2.2 Synthesis of PIM-1 and dinitro compounds for the reduction reaction.

PIM-1 was synthesized via the fast synthetic route reported elsewhere [25-29]. The step growth polycondensation reaction of TTSBI and TFTPN in the presence of excess K_2CO_3 was carried out at 150°C and was completed in 30 minutes. Size exclusion chromatography (SEC) in $CHCl_3$ against polystyrene standards confirmed the apparent weight average molecular weight to be $1.5x10^5$ g/mol. The dinitro derivative of di(ethylene glycol) (DN-EG) was synthesized according to a method as reported in literature [30]. A slightly modified procedure for the synthesis of the bulkier dinitro derivative with PEG 2000 (DN-PEG 2000) was carried out as follows: a mixture of 1-fluoro-4-nitrobenzene and PEG 2000 (molar ratio:1.9:1) was taken in a three necked round bottomed flask fitted with a condenser and argon inlet and stirred in DMF until complete dissolution. Addition of K_2CO_3 to the mixture resulted in a color change from yellow to brown. The reaction mixture was allowed to reflux for 10 days for complete reaction. Removal of the DMF from the mixture resulted in a dark brown sticky solid in 72% yield.

2.3 Preparation of polymer solutions for electrospinning

a. PIM-1 in 1,1,2,2-tetrachloroethane - The PIM-1 polymer solutions with three different concentrations (8, 10 and 12 wt.% with respect to the solvent) were stirred at room temperature overnight to form homogeneous viscous solutions.
b. PAN in DMF- The PAN solutions (8, 10 and 12 wt.% with respect to the solvent) were stirred at 60°C overnight.
c. 6FDA-6FpDA in 1,1,2,2-tetrachloroethane - The 6FDA-6FpDA polymer solutions (8, 10 and 12 wt.% with respect to the solvent) were stirred at room temperature overnight.

2.4 Electrospinning

An electrospinning set up designed and constructed at Helmholtz-Zentrum Geesthacht, Germany, was used to produce fibers from the three different polymer sets. For every set, 2 ml of the viscous polymer solution was drawn in via the syringe needle having an inner diameter

of 0.8 mm. A high voltage power supply was connected to the needle from one end, while an infusion pump pressed the polymer solution out of the needle through the other end. The pump (Medipan Typ 610 BS, Poland) produced a constant flow rate of 1 ml/hr throughout the spinning process. The applied voltage was varied for all the polymer solution sets according to the conductivity of the solution, however, a constant spinning distance of 20 cm (from the needle tip to the collector plate) was maintained for all the polymer sets. The electrospun fibers were collected on the grounded Aluminum foil which rotated at a constant speed of 10 rotations/sec. For all the polymer solutions, the deposition was continued for 1 hour to obtain a dense electrospun mat, which was later detached from the support.

2.5 Immobilization of catalyst on the surface of the nanofibers

An area of 3 x 7 cm^2 10 wt.% PIM-1 electrospun mat containing the support was cut out from the big cylindrical roll of spun fibers . The rectangular piece was then dipped in a solution containing varying amounts of $PdAc_2$ dissolved in 16 ml ethyl acetate (EtAc) and 8 ml ethanol (EtOH). The details of the compositions of the fibers and their coating concentrations are provided in Table 1.

Table 1. Compositions of the electrospun polymers with their Pd loading

Batch	Electrospun Polymer	Conc.of polymer (wt.%)	Conc. of $PdAc_2$ for coating the fibers (wt.%)	Relative Pd content on the fibers [a)] (%)	Voltage of electrospinning (kV)
A	PIM-1	10	0.1	2.6	15.0
	PIM-1	10	0.25	3.3	15.0
	PIM-1	10	0.5	3.9	15.0
	PIM-1	10	1.0	4.6	15.0
B	PIM-1	8	0.25		14.0
	PIM-1	10	0.25	3.3	15.0
	PIM-1	12	0.25		18.2
	PAN	8	0.25		16.5
	PAN	10	0.25	3.5	20.5
	6FDA-6FpDA	8	0.25		15.2
	6FDA-6FpDA	10	0.25	0.7	19.2
	6FDA-6FpDA	12	0.25		20.4

[a)] The relative Pd contents were calculated from the rest masses of the Pd coated and the pure fibers. (see Supporting Information S1)

Batch A deals with PIM-1 fibers spun from 10 wt.% concentration and then coated with solutions containing 0.2 g (1 wt.%), 0.1 g (0.5 wt.%), 0.05 g (0.25 wt.%) and 0.025 g (0.1 wt.%) $PdAc_2$ in EtAc:EtOH (2:1), respectively. Batch B deals with PIM-1, PAN and 6FDA-

6FpDA fibers spun from different concentrations and then coated with 0.25 wt.% $PdAc_2$. Since EtAc is a solvent for the 6FDA-6FpDA, the $PdAc_2$ solution for this polymer was prepared in EtOH only. The nanofiber mats were first dipped in the corresponding clear orange $PdAc_2$ solution (1 min), then removed from the solution and dried in air for 1 hr. This was followed by transferring the coated fibers in an oven heated at 150°C overnight.

2.6 Test of catalytic activity: reduction of *p*-nitrophenol

The Pd coated electrospun PIM-1, PAN and 6FDA-6FpDA fibrous mats were initially isolated from the support material. A similar amount of the coated polymer fibers was weighed in six different glass vials. Aqueous $NaBH_4$ solution [10 g/L] which served as the reductant for the conversion of *p*-nitrophenol to *p*-aminophenol was then added to the vials under constant stirring. This was followed immediately by the addition of the *p*-nitrophenol [0.02 g/L] solution and the timer was started, to monitor the catalytic reduction of the *p*-nitrophenol solution. The progress of the catalytic conversion was manifested in its absorption spectra which were recorded in a TU-8110 UV-Vis spectrophotometer (Kyoto, Japan). Samples were recorded every 3 min for a period up to 15 min for the completion of the reduction process. The standard quartz cell in which the catalytic reduction was conducted had a path length of 1 cm.

2.7 Characterization

The ^{1}H NMR spectrum in $CDCl_3$ were recorded on a Bruker AV500 spectrometer (Karlsruhe, Germany) operating at 500MHz using a 5 mm $^{1}H/^{13}C$ TXI probe at a sample temperature of 25°C (298 K). ^{1}H spectra were recorded applying a 10 ms 90° pulse.

The molecular weight of PIM-1 was measured by a gel-chromatograph (Polymer Standards Service GmbH, Mainz, Germany) using a column combination [precolumn SDV-linear, SDV linear and SDV-102 nm] at a flow rate of 1.0 ml/min. The apparent molecular weight evaluation was done with a combination of refractive and UV detectors, where THF was used as the eluent and polystyrene (PS) as the calibration standard.

Characterization of the electrospun fibers was performed using a Merlin scanning electron microscope (Zeiss, Oberkochen, Germany) operated between 1-1.5 KV. Samples were sputtered with a 2 nm thick layer of Pt. The catalytically active nanofibers were coated with carbon prior to analysis.

The cross section of the fibers were analyzed with a transmission electron microscope (TEM) Tecnai G^2 F20 from FEI (Eindhoven, The Netherlands) operated at 120 kV. The electrospun fibers were embedded in Epotek 301 and ultrathin cuts were analysed without any

further treatment. The diameter and standard deviation of 20 fibers distributed over the micrograph were measured with the Software IMS, Imagic Bildverarbeitung AG.

Detection of the Pd nanoparticles was also done by X-ray diffraction (XRD) using a Bruker D8 Discover X-ray diffractometer (Karlsruhe, Germany) with copper radiation (Cu, Kα, 50kV, 40mA) and a VANTEC 2D detector. Air tight sample holders were used to prevent contamination of the samples. A piece of mat was placed onto the sample holder and was scanned over more than 20 times to improve the signal-noise ratio of the data. Data were collected at room temperature between 20 and 97.5° (2θ) with the speed of 1° min^{-1}. The diffraction images were integrated with the DIFFRAC. EVA software provided by Bruker.

2.8 Sorption experiments

In order to determine the adsorption of *p*-nitrophenol, DN-EG, DN-PEG 2000 on the polymers PIM-1, PAN and 6FDA-6FpDA, a series of sorption or swelling tests were performed. For *p*-nitrophenol, 0.02 g of each of the polymers were suspended in three different glass vials containing 15 ml of 0.02 g/L aqueous *p*-nitrophenol solution. The solutions were stirred and samples of 1 ml were withdrawn and measured in the UV-Vis spectrophotometer. This process was continued up to 4 hours for the sorption process to be near to completion. In the case of the dinitro compounds, the process was repeated with the similar amount of polymer suspended in 15 ml of 0.05 g/L and0.323 g/L of DN-EG and DN-PEG 2000 respectively dissolved in acetonitrile, respectively.

3 Results and discussion

3.1 Synthesis of dinitro derivatives

The dinitro derivative with PEG 2000 was synthesized using two methods with slight modifications to the already reported method of synthesis of dinitro derivatives [30]. In the first method an excess (2.3 times) of the 1-fluoro-4-nitrobenzene with respect to the PEG 2000 was reacted with K_2CO_3 under argon atmosphere. Although this method led to the complete conversion of the PEG 2000 to the dinitro derivative, the excess 1-fluoro-4-nitrobenzene was difficult to be isolated from the product. In order to prevent the Pd particles from catalyzing the reduction of excess 1-fluoro-4-nitrobenzene to its corresponding amino compound, it was important to minimize the amount of the 1-fluoro-4-nitrobenzene in the product. Therefore in the second method (Scheme 1), the 1-fluoro-4-nitrobenzene was deficient (1.9 times) with respect to the PEG 2000, while the similar amount of K_2CO_3 was maintained as before. This method resulted in an excess of PEG 2000 along with a slight excess of 1-fluoro-4-nitrobenzene. Since PEG 2000 did not take part in the catalytic reaction, and the unreacted 1-

fluoro-4-nitrobenzene was negligible, therefore the second method was chosen for the synthesis of the dinitro derivative with PEG 2000. The compound was characterized by ^{1}H-NMR spectroscopy.

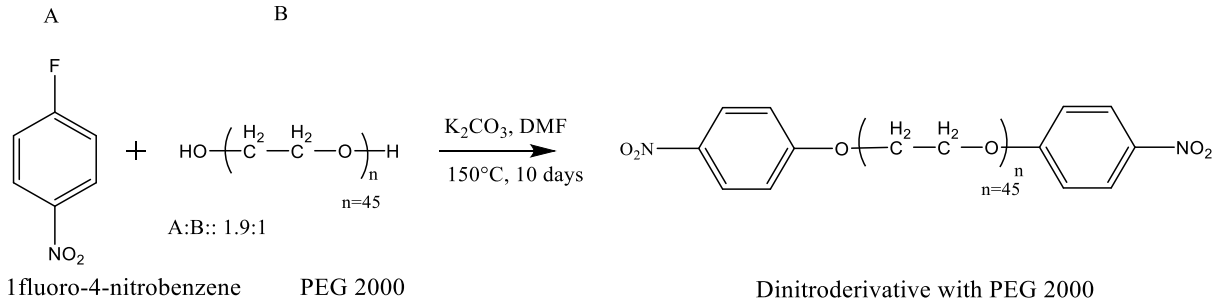

Scheme 1 Reaction route: Synthesis of dinitro derivative with PEG 2000

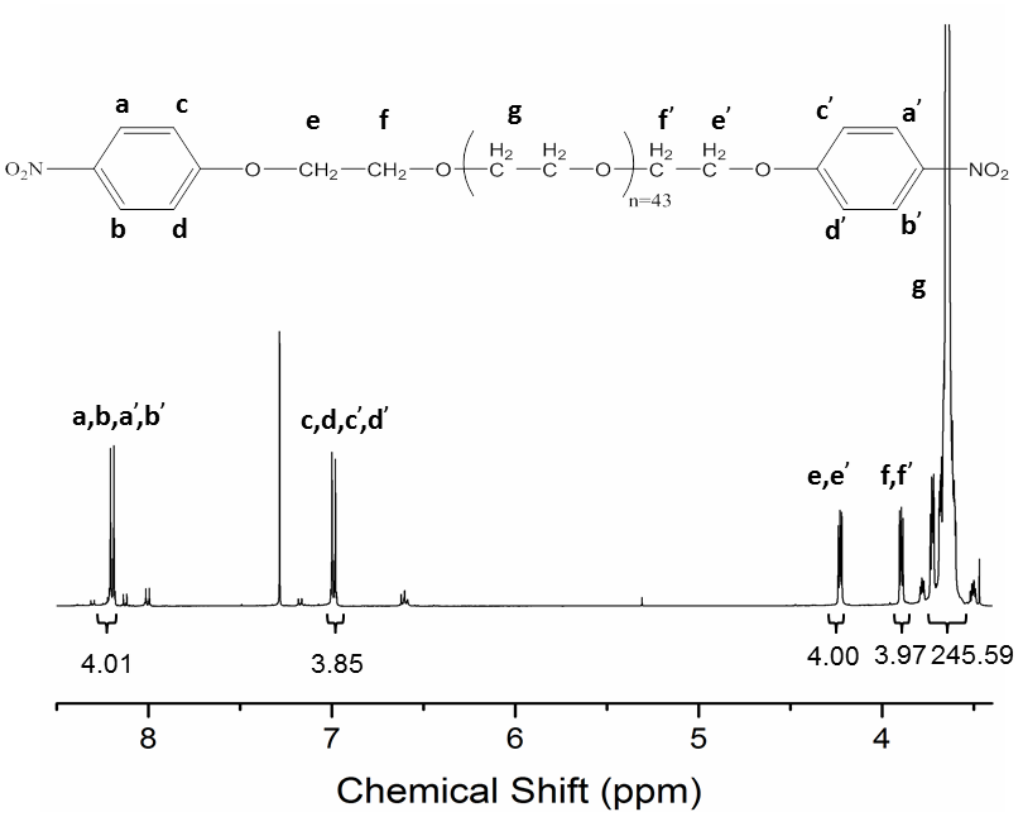

Figure 1. ^{1}H-NMR spectrum of DN-PEG 2000 derivative in $CDCl_3$

Fig. 1 shows the ^{1}H-NMR spectrum of the DN-PEG 2000 with the allocation of protons. The ^{1}H signals corresponding to the four aromatic protons of the benzene containing the $–NO_2$ group are observed at 8.21 and 8.19 ppm. The other characteristic aromatic protons being in the vicinity of the ethylene glycol groups are shifted slightly towards lower ppm values and appear at 7.01 and 6.98 ppm. Out of the 45 ethylene glycol units of PEG 2000, only two of them have

different electronic environments due to the terminal nitrobenzene rings, and appear at 4.23 and 3.89, respectively. The remaining –OCH_2 groups of the PEG 2000 along with some excess PEG from the synthesis exhibit a strong signal around 3.63 ppm.

3.2 Results of electrospinning

3.2.1 Electrospinning of PIM-1

1,2-dichlorobenzene was initially chosen as the solvent for electrospinning PIM-1 owing to its higher boiling point compared to all the other solvents for PIM-1. However, electrospinning with 8, 10 and 12 wt.% PIM-1 in dichlorobenzene resulted in agglomerated fibers, appearing in a gel like mass, which occurred probably due to the very high boiling point (180.5°C) of the solvent resulting in insufficient drying of the fibers prior to reaching the collector. Additionally, the formation of beads throughout the fiber network for all the concentration range confirmed the difference in solubility parameters between the PIM-1 and solvent molecules [31]. On account of these difficulties 1,1,2,2-tetrachloroethane [19-21] was used as the solvent for electrospinning PIM-1. The PIM-1 powder was dissolved in 1,1,2,2-tetrachloroethane (8, 10 and 12 wt.%) and allowed to stir overnight for sufficient entanglements between the chains inducing fiber formation. The beaded morphology decreased while the fiber diameter increased, when the polymer concentration was increased from 8 to 12 wt.% (Fig.2).

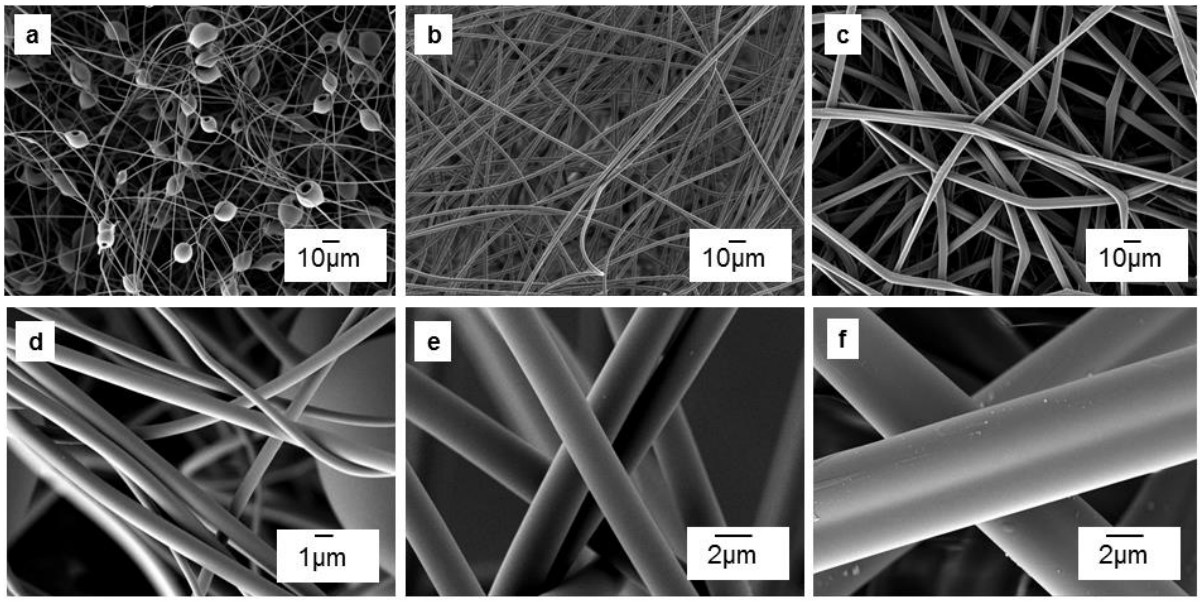

Figure 2. SEM images of PIM-1 solutions with different concentrations (a) 8 wt.%, (b) 10 wt.% and (c) 12 wt.% in 1,1,2,2 tetrachloroethane. Figs. 2(d), (e) and (f) represent details of Figs. 2a, b and c, respectively.

3.2.2. Electrospinning of PAN

The fibers generated from the 8 and 10 wt.% solutions of PAN in DMF are smaller in diameter than the PIM-1 fibers in 1,1,2,2-tetrachloroethane. Concentrations lower than 8 wt.% resulted in a mixture of beads and fibers owing to low viscosity and high surface tension of the solution [32], while a concentration higher than 10 wt.% resulted in a solution too viscous for electrospinning, therefore 2 sets of fibers with different diameters from 10 wt.% were generated by application of different voltages (17 kV and 20 kV). Nevertheless, the fibers made from 8 and 10 wt.% were found to be smooth and uniform and had a higher density than the PIM-1 fibers (Fig. 3).

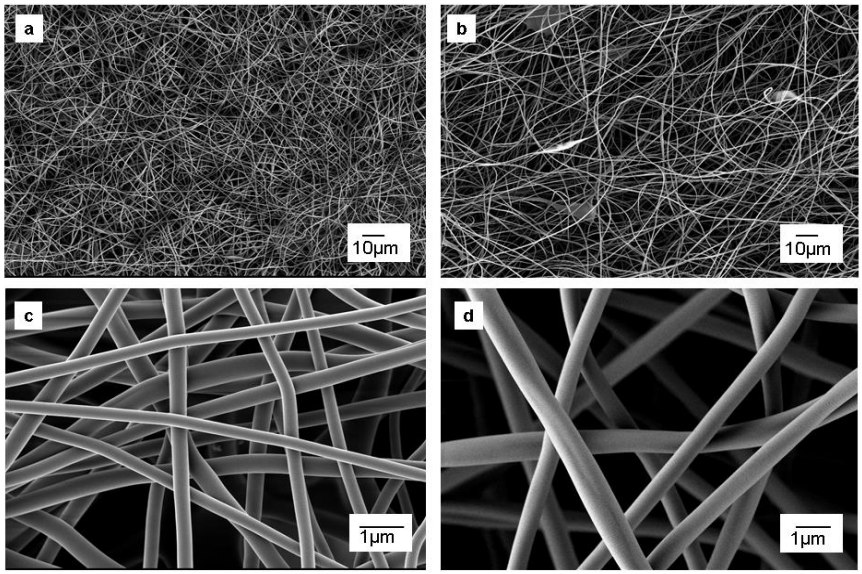

Figure 3. SEM images of the PAN solutions with different concentrations (a) 8 wt.% and (b) 10 wt.% in DMF respectively. Fig. 3 (c) and (d) show details of Fig. 3a and 3b, respectively.

3.2.3. Electrospinning of 6FDA-6FpDA

The fibers produced from the 6FDA-6FpDA solutions (8, 10 and 12 wt.% in 1,1,2,2-tetrachloroethane) have the least diameter compared to PAN and PIM-1 fibers. The formation of beads in all the 6FDA-6FpDA fibers can be attributed to the lower viscosity of solutions, which results in poor polymer chain entanglements and hence instability of the polymer jet.

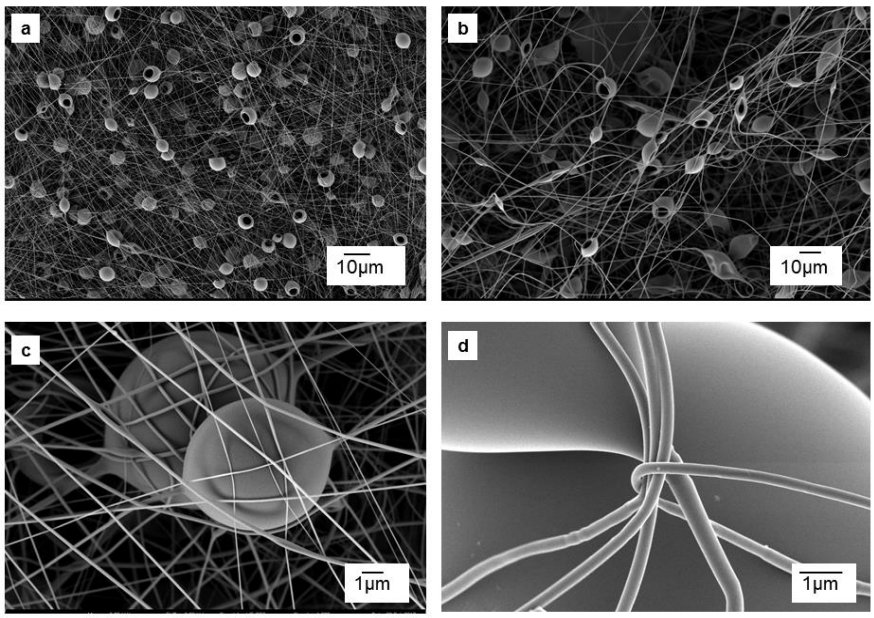

Figure 4. SEM images of the 6FDA-6FpDA solutions with different concentrations (a) 8wt.% and (b) 12 wt.% in 1,1,2,2-tetrachloroethane. Fig. 4c and d show details of Fig. 4a and 4b, respectively.

3.3. Preparation and Characterization of Pd nanoparticles

Samples of catalytically activated polymers were obtained by coating the electrospun fibers (e.g. 10 wt.% PIM-1) with 0.1 w%, 0.25 wt.%, 0.5 wt.% and 1 wt.% $PdAc_2$ solution with respect to EtAc/EtOH (2:1). It is assumed that PIM-1 swells in the solvents (especially in EtOH) [33] and by this way the $PdAc_2$ is transported into the fibers. The PAN and 6FDA-6FpDA fibers were also coated in the similar manner but only with 0.25 wt.% $PdAc_2$. In the case of 6FDA-6FpDA only EtOH was used for dissolving the $PdAc_2$, since EtAc served as a solvent for the polymer. The reduction from the $PdAc_2$ to the catalytically active metal is started by ethanol, and later firmly embedded on the surface of the nanofibers by a thermal treatment. A solution of $PdAc_2$ in ethanol is changing its colour from orange to grey/black rather fast, because of the ongoing reduction from Pd^{2+} to Pd which is precipitating. Therefore, the dipping of the 6FDA-6FpDA fiber mat was performed as soon as the solution was clear orange; however, some slight reduction of Pd^{2+} must have already occurred, causing the obtainable Pd content of 6FDA-6FpDA fibers to be lower than in the other polymers (Table 1).

Concentration of Pd in the activated fibers was measured by TGA (see Supporting Information S1): When the PIM-1 and the Pd coated PIM-1 fibers are subjected to thermal degradation, the PIM-1 polymer is completely degraded to carbon at 800°C while Pd stays unchanged. A comparison of the pristine fibers with the corresponding coated fibers allows the estimation of

the actual Pd content.

The Pd nanoparticles embedded mostly on the surface of the electrospun fibers were imaged by scanning electron microscopy and also detected by XRD. Cross sections of the fibers were studied by TEM to determine the dispersion of the PdNPs on the outer and inner surface of the electrospun fibers.

The SEM shows the activated PIM-1 fibers with a smooth surface by using secondary electrons for imaging (Fig. 5a-c). The back scattered electron image (BSE) which is used to detect the contrast between areas with different chemical compositions, shows the PdNPs as bright spots (Fig. 5d and e). This is because the heavy Pd back scatters electrons more strongly than the lighter elements constituting the PIM-1 polymer.

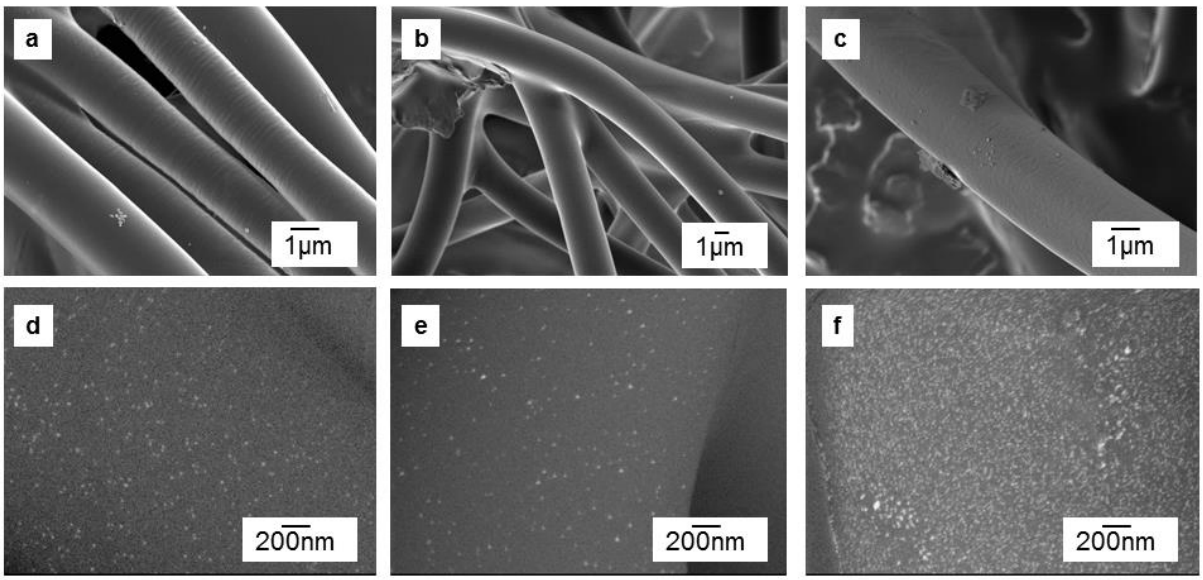

Figure 5. The secondary electron images of the surface of the electrospun PIM-1 (10 wt.%) coated with (a) 3.3 wt.%, (b) 3.9 wt.% and (c) 4.6 wt.% Pd. The BSE images of the similar electrospun polymer activated by (d) 3.3 wt.%, (e) 3.9 wt.% and (f) 4.6 wt.% Pd are shown in the second row.

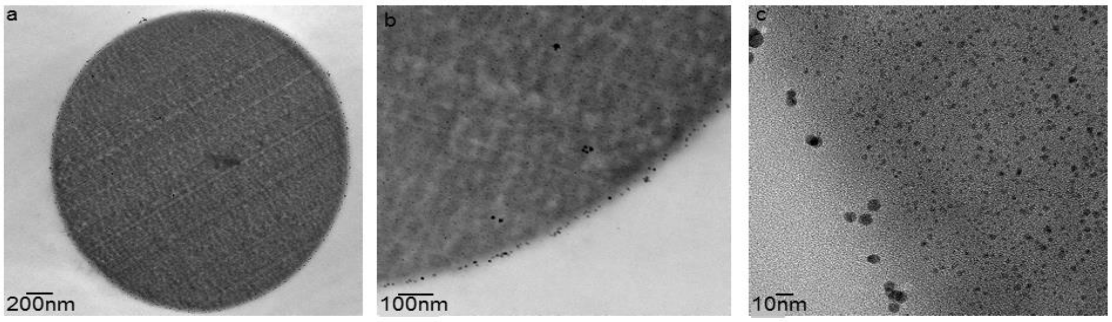

Figure 6. TEM image of the cross section of the (a) electrospun PIM-1 (10 wt.%) fiber, (b) the outer surface in higher magnification and (c) the dispersion of the particles at the surface showing some agglomerate formation. The fiber has a Pd content of 4.6 wt.%.

The distribution and the excess dispersion of the PdNPs on the surface of the fibers were estimated from the TEM images (Fig. 6). The distribution of the particles on the inner surface of the fibers confirms that the catalytic activity is contributed by the PdNPs not just on the surface of the fibers but also by the nanoparticles located inside the fibers. A comparative TEM study on the PAN and 6FDA-6FpDA fibers shows clearly that the Pd nanoparticles are located on the surface of these fibers only (see Supporting Information S2).

The X-ray diffraction pattern of the PIM-1 fibers with and without PdNPs is illustrated in Fig. 7. The broad peak appearing around $2\theta = 40.1°$ corresponds to the (111) peak of Pd with an fcc structure. The broad peak also indicates a small size of the crystalline nanoparticles. However, determination of the Pd crystal size was impossible from the XRD data because of the non-uniform baseline leading to inappropriate fitting of the Gaussian curve for a full width at half maximum estimation.

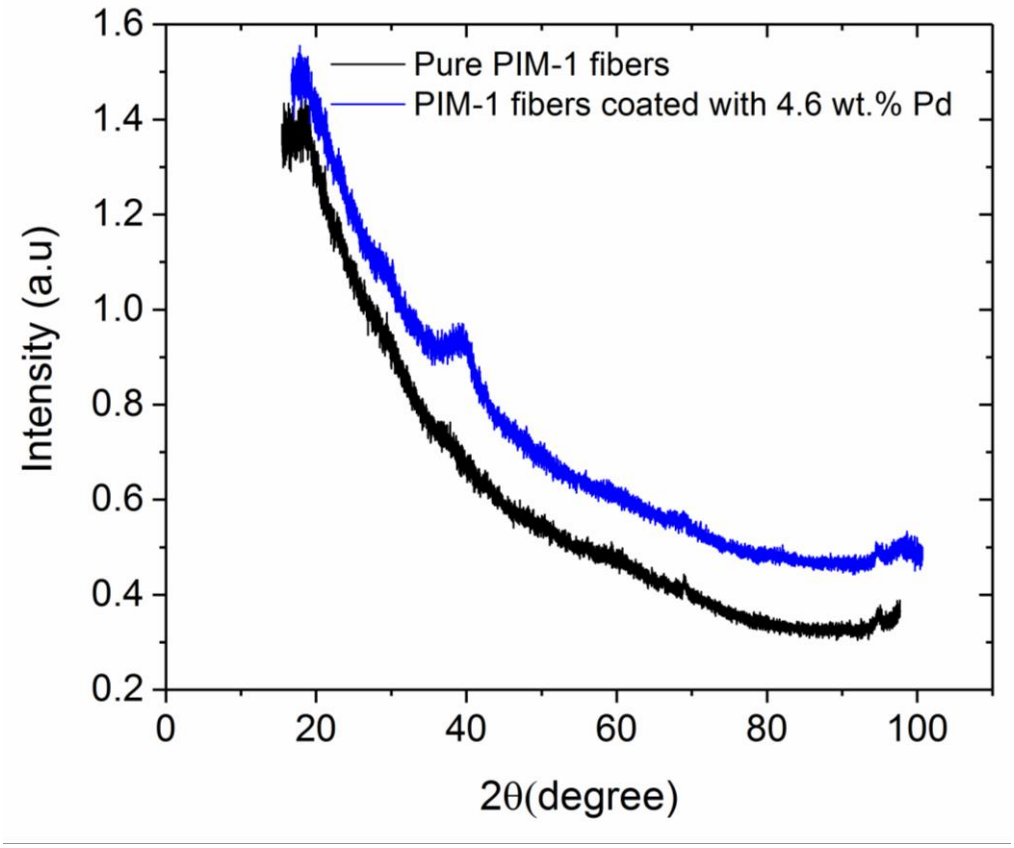

Figure 7. X-ray diffraction images of the PIM-1 fibers with and without Pd nanoparticles

3.4. Catalytic activity of Pd embedded on the electrospun fibers

The catalytic activity of the Pd nanoparticles embedded on the electrospun PIM-1 fiber mat was demonstrated by the reduction of *p*-nitrophenol to *p*-aminophenol with $NaBH_4$ which is, as mentioned before, a standard reduction reaction for studying the catalytic activity of transition metals [22, 23]. Before starting the reaction, a calibration of the concentration of of *p*-nitrophenol was made by recording the absorbance of *p*-nitrophenol at different concentrations as a function of wavelength (see Supporting Information S3).

The reduction reaction was studied by drawing 1 ml of the *p*-nitrophenol aqueous solution in the cuvette in intervals of 3 min and recording its absorption intensity as a function of wavelength. Fig. 8 shows the process of *p*-nitrophenol reduction at different times for varied contents of Pd loading on the electrospun PIM-1 (10 wt.%) fibers.

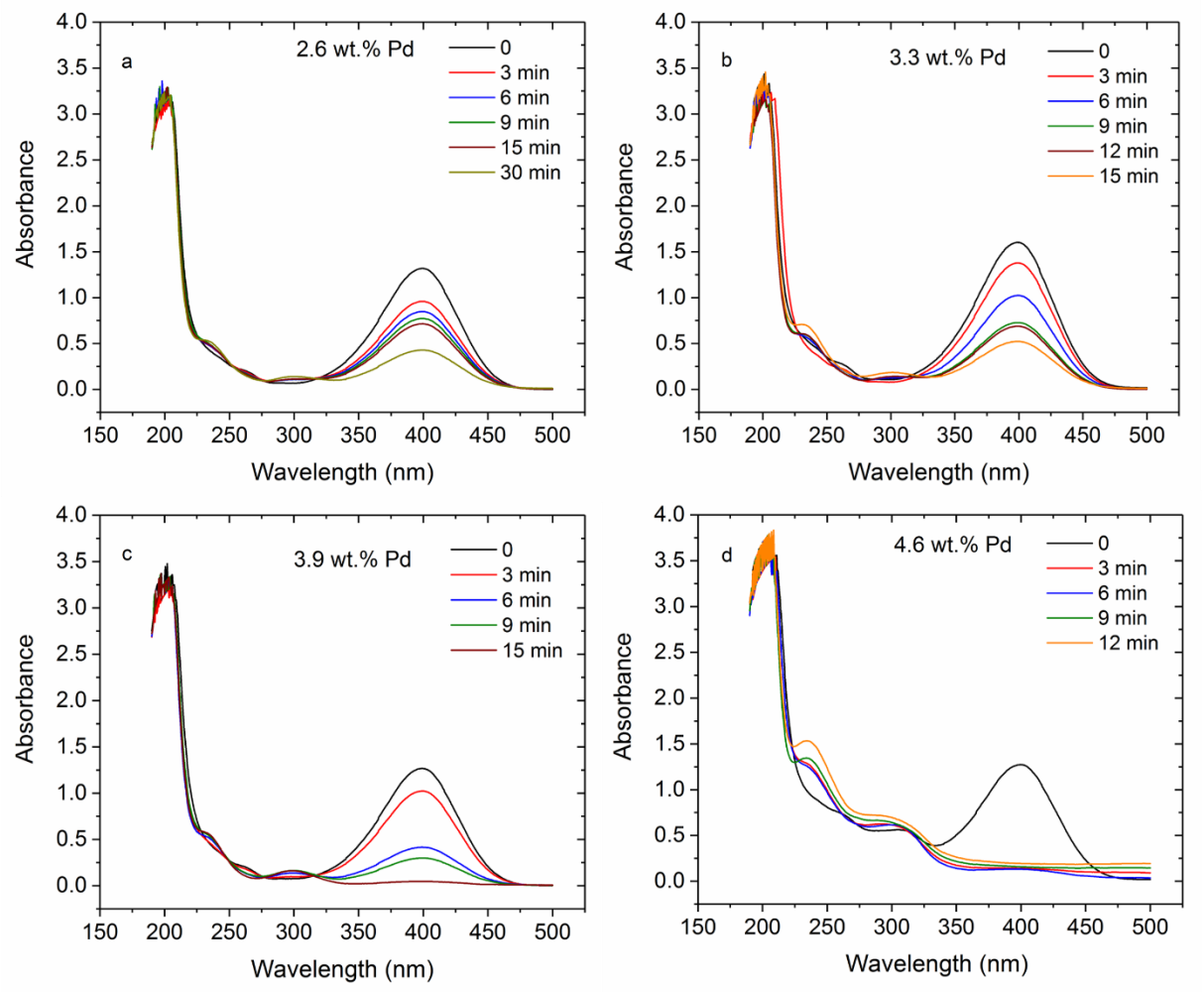

Figure 8. UV/Vis spectra of an aqueous solution of *p*-nitrophenol (0.02 g/L) and $NaBH_4$ (10g/L) treated by immersing electrospun PIM-1 fibers with a) 2.6, b) 3.3, c) 3.9 and d) 4.6 wt.% Pd . All experiments have been conducted at 25°C.

The intensity of the characteristic peak at 400 nm, representative of *p*-nitrophenol, is found to decrease while that at 310 nm, characteristic of the product *p*-aminophenol, is found to increase with time. The rate of decrease of *p*-nitrophenol and the concurrent increase of the *p*-aminophenol gets enhanced with increasing content of Pd on the fiber.

Comparison of the calibration curve of *p*-nitrophenol with that of different contents of PdNPs embedded on the electrospun fibers implies that 50%, 75%, and 100% of the *p*-nitrophenol conversion occurred for the 2.6, 3.3 and 3.9 wt.% Pd within 15 min. However, for the sample with 4.6 wt% Pd, 100% conversion occurs within 3 min. The catalytic efficiency of the Pd nanoparticles supported by the electrospun PIM-1 fibers was found to be in the range of 130-170 mmoles $L^{-1}hr^{-1}$ mg^{-1} Pd. The reusability of the Pd particles on PIM-1 was tested in 3

reduction cycles and was found to yield the same catalytic conversion (from *p*-nitrophenol to *p*-aminophenol) (see Supporting Information S4).

In order to determine the exact rate of the reduction reaction, it was necessary to express the exponent to which its reactant term in the rate equation is raised, or in other words, to estimate the order of the chemical reaction. In this reaction, the $NaBH_4$ content greatly exceeds the content of *p*-nitrophenol, so the rate of reaction can be treated as independent or as pseudo zero order with respect to $NaBH_4$ concentration. The ratio of absorbance of A_t of *p*-nitrophenol at time t, to its value A_0 at t = 0, A_t/A_0 directly gives the concentration ratios, C_t/C_0 of *p*-nitrophenol. Thus the kinetic equation of the reduction reaction could be expressed as,

$A_t = A_0 - kt$ (1) zero order reaction

$A_t = A_0 \exp(-kt)$ (2) 1st order reaction

$1/A_t = 1/A_0 + kt$ (3) 2nd order reaction

However, for all the different Pd concentrations (except the sample with 4.6 wt.% Pd content where the entire catalytic conversion gets completed in three minutes), the plot of ln A_t/A_0 versus time t (Fig. 9 a) was found to be a straight line with negative slope, indicating that the reduction of *p*-nitrophenol to *p*-aminophenol is a first order reaction with respect to the *p*-nitrophenol concentration. The rate constants for all the different amounts of PdNPs resulting from the applied solutions with different concentrations of $PdAc_2$ were determined directly from the slope of the best linear fit, following a first order kinetics (equation (2)).

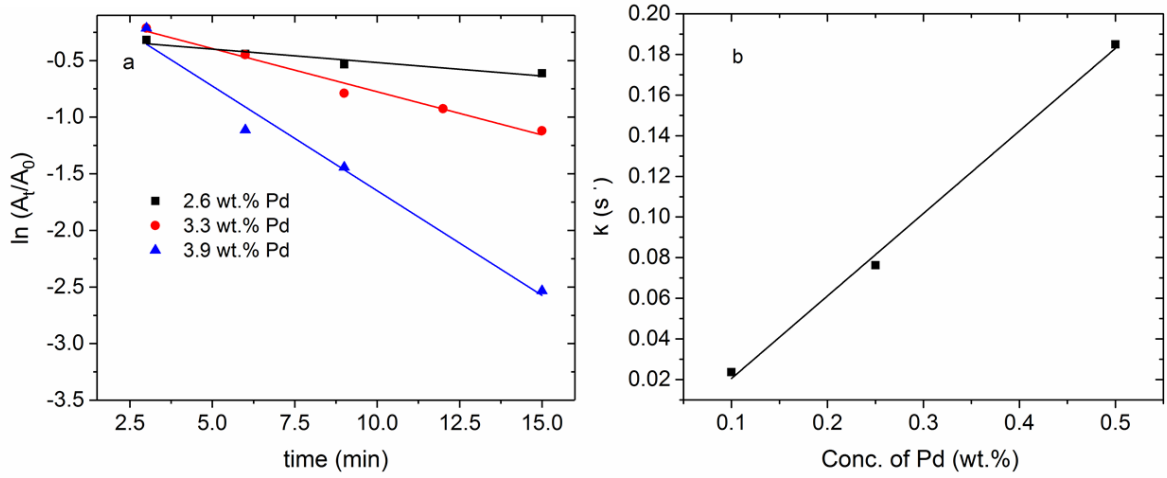

Figure 9. The plot of a) ln A_t/A_0 versus time and b) rate constant versus concentration for the reduction reaction of *p*-nitrophenol catalyzed by different concentrations of Pd embedded on the electrospun PIM-1 fibers. The reaction conditions are as follows: [*p*-nitrophenol]: 0.02

g/L; [$NaBH_4$]: 10 g/L; T: 25°C; Solvent: Water.

It was found from Fig. 9b that there is a linear increase of the rate constant with the increase in the Pd concentration. The similar experiment was repeated with the *p*-nitrophenol in the presence of $NaBH_4$ (without the PdNPs embedded on PIM-1 fibers), and it was found that there was no decrease of the *p*-nitrophenol concentration with time, indicating that the reduction reaction is activated only in the presence of Pd composites in the system. Reaction progress was also monitored with just the PIM-1 fibers, and only 5% of the *p*-nitrophenol content decreased with time (15 min) with no appearance of the *p*-aminophenol peak. However, since this decrease was much smaller as compared to the reduction with Pd nanoparticles on the fiber, it could be attributed to the absorption of PIM-1 of *p*-nitrophenol as it was already manifested in the pervaporation characteristics of phenol [34] through the highly permeable PIM-1.

Since temperature has an important influence on most chemical reactions, the effect of temperature on the reduction reaction of *p*-nitrophenol was studied at four different temperatures (20°C, 30°C, 40°C and 50°C). The plots of ln A_t /A_0 versus time for these four temperatures are shown in Fig. 11a.

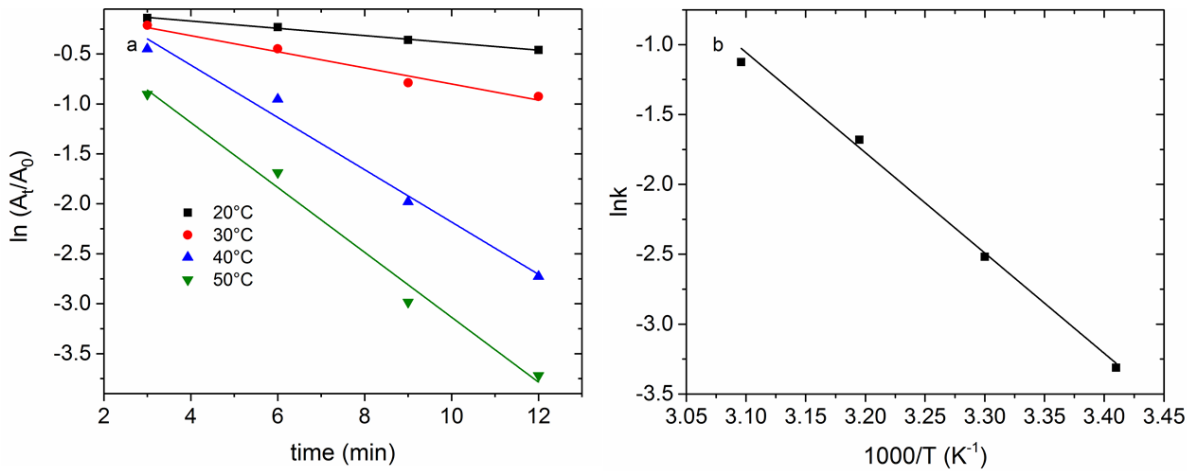

Figure 10. The plots of a) ln A_t/A_0 versus time at different temperatures b) Arrhenius plot for the reduction reaction of *p*-nitrophenol. The reaction conditions are as follows: [*p*-nitrophenol]: 0.02 g/L; [$NaBH_4$]: 10 g/L; Solvent: Water; T: 25°C.

The linear functions in Fig. 10a confirm the first order kinetics observed for all temperatures. The rate constants for the four temperatures were calculated directly from the slopes of the linear plots. The increase of the rate constant with the increase in temperature (Fig. 10b) shows that the temperature had a direct influence on the reduction reaction and can be expressed by the Arrhenius equation,

$$k = A \exp(-E_a/RT) \qquad (4)$$

where k is the rate constant, A is an Arrhenius constant, E_a is the activation energy of the reaction, R is the universal gas constant and T is the absolute temperature.

The activation energy calculated from the slope of the Arrhenius plot (Fig. 10b) was 60 kJ/mol. This value was found to be in good agreement with the literature reported value (61 kJ/mol) for the catalytic hydrogenation of *p*-nitrophenol to *p*-aminophenol [35].

4. Comparison of the reduction performance of PIM-1 with other polymer supports

The high sorption of the *p*-nitrophenol in PIM-1 and large surface area of the fibers were considered to be the driving force for the high catalytic efficiency. For an effective comparison of the catalytic behavior of the PIM-1 support, a study of the similar catalyst driven reduction reaction (*p*-nitrophenol to *p*-aminophenol) was carried out using PAN and 6FDA-6FpDA electrospun fibers as supports for PdNPs by using the similar procedure as used for the PIM-1 nanofiber supported PdNPs (Table 1, Batch B). The variation of the rate constant with fiber diameter helped to determine the influence of the *p*-nitrophenol sorption and fiber diameter on the catalytic efficiency or the rate constant (Fig. 11).

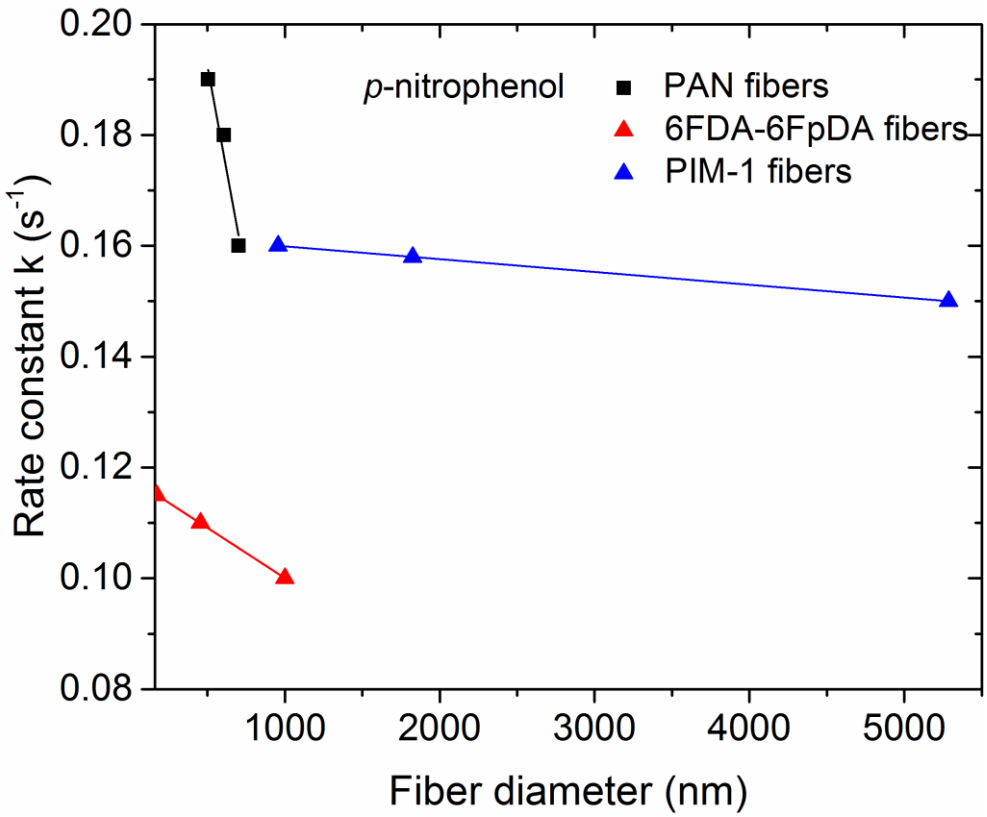

Figure 11. Graph showing the change of rate constant with fiber diameter for three different sets of PIM-1 (8, 10, 12 wt.% PIM-1 in spinning solutions, with approx. 3 wt.% PdNPs content), PAN (8 and 10 wt.% (2 fiber mats prepared by different voltages, with approx. 3 wt.% PdNPs) and 6FDA-6FpDA fibers (8, 10, 12 wt.%, with approx. 1 wt.% PdNPs). The reaction conditions are as follows: [*p*-nitrophenol]: 0.02 g/L; [$NaBH_4$]: 10 g/L; Solvent: Water; T: 25°C.

The nearly constant slope of the rate constant versus fiber diameter for the PIM-1 fibers can be attributed to the high sorption characteristics of PIM-1 for phenols, in our case, *p*-nitrophenol (Fig. 12 a). The adsorption of *p*-nitrophenol into PIM-1 over time is clearly visible from the decrease of the aromatic -NO_2 absorbance at 325 nm. The high sorption properties of PIM-1 for phenols from water have also been observed in earlier pervaporation studies [34], where the permeate was enriched in phenol up to ten-fold demonstrating the organophilic character of the membrane. Therefore, despite changing the fiber diameter of PIM-1 to a significant extent, its rate constant does not change proportionally (Fig. 11).

PAN is more hydrophilic than PIM-1 and 6FDA-6FpDA, and correspondingly also exhibits some adsorption of the *p*-nitrophenol from aqueous solution (Fig. 12 b). However, in

addition to the decrease of the aromatic NO_2 peak, there is an appearance of a new peak at 400 nm. Such an observation can be explained by the formation of a charge transfer complex between the cyano groups of the polyacrylonitrile with the nitro groups of the *p*-nitrophenol. In the case of PIM-1, such an effect is not observed because the cyano groups are in conjugation with the aromatic backbone and therefore not available for the formation of any complex with other moieties. Therefore, the sorption and chemical interaction of PAN with *p*-nitrophenol, combined with its low fiber diameter explains its very high rate constant (Fig. 11).

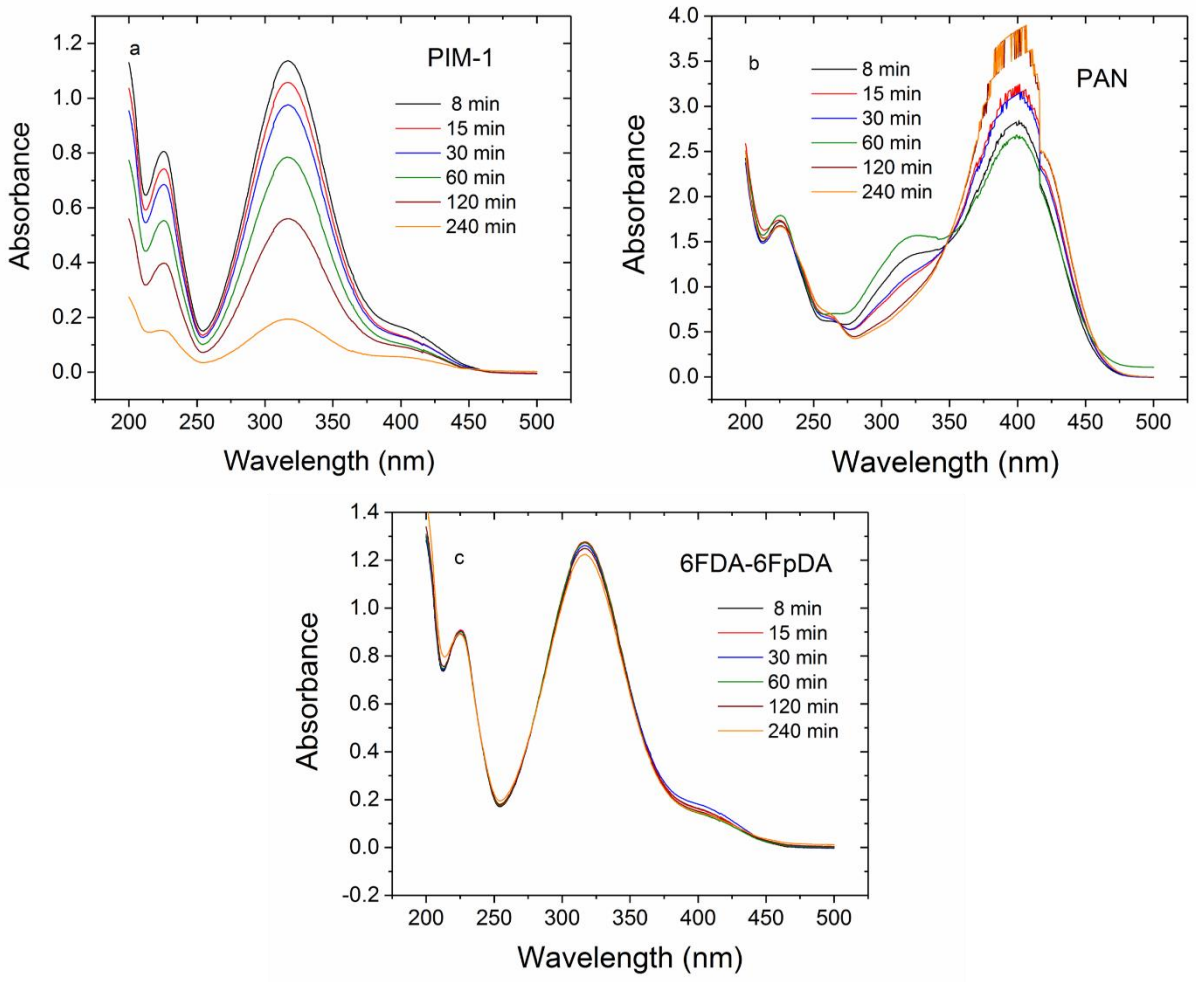

Figure 12. Sorption studies of pristine fibers mats of a) PIM-1, b) PAN and c) 6FDA-6FpDA in aqueous solution of [*p*-nitrophenol]: 0.02 g/L.

In comparison to PAN and PIM-1, the 6FDA-6FpDA polyimide is a relatively more hydrophobic material [37] and is found to have negligible swelling effect (Fig. 12 c) compared

to the other two polymers. The very low rate constant of the polyimide therefore depends only on its fiber diameter.

In the former comparative study, it was determined that the sorption of the small *p*-nitrophenol molecule into PIM-1 and PAN was primarily responsible for their high catalytic activity compared to the 6FDA-6FpDA polymer. In order to give further evidence for this interpretation, the above process was repeated with two bulky nitrocompounds (DN-EG) and DN-PEG 2000. The experiments were carried out similar to the above comparative study, except the necessary change of the solvent system. Instead of water, a mixture of acetonitrile: water (1:1) was used in this case because the dinitro compounds do not dissolve in water.

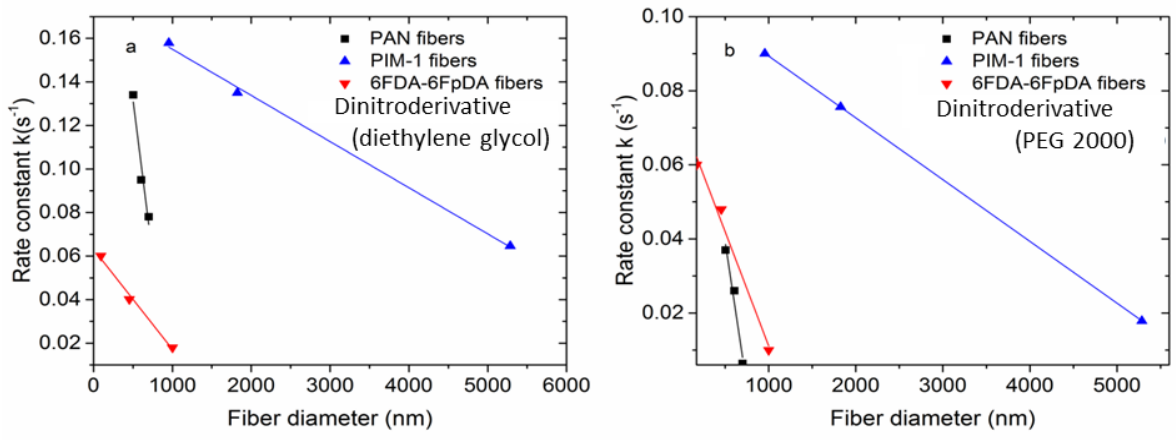

Figure 13. Graph showing the change of rate constant with fiber diameter for the reduction of (a) dinitro derivative (diethylene glycol) and (b) dinitro derivative (PEG 2000). In each case three different sets of PIM-1 (8, 10, 12 wt.% PIM-1 in spinning solutions, with approx. 3 wt.% PdNPs content), PAN (8 and 10 wt.% (2 fiber mats prepared by different voltages, with approx. 3 wt.% PdNPs) and 6FDA-6FpDA fibers (8, 10, 12 wt.%, with approx. 1 wt.% PdNPs) were considered. The reaction conditions are as follows: 13a. [Dinitro derivative (diethylene glycol)]: 0.05 g/L; [$NaBH_4$]: 20 g/L; Solvent: Acetonitrile: Water: 1:1; T: 25°C. 13b. [Dinitro derivative (PEG 2000)]: 0.323 g/L; [$NaBH_4$]: 130 g/L; Solvent: Acetonitrile:Water: 1:1; T: 25°C.

Similar swelling experiments were conducted on both the dinitro compounds, however no significant adsorption of the compounds by the polymers could be observed. Therefore the catalytic behavior in this case could be considered to be a factor of the specific surface area of

the fibers and availability of the compounds by the catalysts. Overall, the rate constants for the reduction of both the dinitro compounds are lower in comparison to the reduction of *p*-nitrophenol (Fig. 13). Such an observation can be related to the reduced mobility of the bulky dinitro compounds (even more pronounced for the DN-PEG 2000and the hence lesser availability of the compound to the catalyst nanoparticles. In the absence of any sorption effects, the PIM-1 with the lowest fiber diameter was found to exhibit the highest rate constant which can be attributed to its high specific surface area. The rate constant for both the PAN and PIM-1 fibers decreases on changing the dinitro compound from diethylene glycol to PEG 2000. However; the 6FDA-6FpDA fibers do not exhibit such a proportional decrease which can be explained by the hydrophobic character of 6FDA-6FpDA. The hydrophobicity of the polyimide might prevent the interaction of the polymer with the different groups on the dinitro compounds which results in no significant change in the rate constants.

5. Conclusion

This work demonstrated successfully the applicability of smooth and uniform electrospun polymeric fibers made from PIM-1 as a superior catalyst supporting material due to their high surface to weight ratio. This was demonstrated by comparing electrospun PIM-1 fibers with similarly prepared fibers from two other polymerers, namely PAN and 6FDA-6FpDA. The electrospun fibers were catalytically activated by coating with palladium diacetate in an organic solution, followed by a thermal treatment in air, to embed the nanosized Pd catalyst on the surface of the fibers. The catalytic activity of the Pd coated fibers was tested by the standard reduction of *p*-nitrophenol to *p*-aminophenol. Temperature and concentration of the palladium catalysts were found to be the prime factors controlling the rate of the first order reduction reaction. The rate constant of the PIM-1 fibers was found to remain constant with the fiber diameter while that of 6FDA-6FpDA and PAN fibers decreased with increasing fiber diameter respectively lower surface area. This indicates that the catalytic reactions take place not only on the outer surface of the fibers, but also on the inner surface in the case of PIM-1 due to the intrinsic microporosity allowing the PIM-1 fibers to sorb the Pd salt solution (leading to the catalytic PdNPs during activation) and also to sorb not too large reactants such as *p*-nitrophenol. This shows the superiority of PIM-1 fiber mats as support material for catalytic nanoparticles. For larger reactants, the catalytic reactions mainly occur at the fiber surface, which also indicates in principle size selectivity for these reactants. However, also in the case of reduction of larger reactants like the dinitro compounds containing varying PEG chain lengths which

cannot penetrate into the PIM-1 fibers, they also outperformed PAN and 6FDA-6FpDA supports.

Acknowledgement

The authors would like to thank Dr. Alberto Tena for the synthesis of 6FDA-6FpDA polyimide. Clarissa Abetz is kindly acknowledged for helpful discussions and the TEM measurements. Anke-Lisa Metze is kindly acknowledged for the SEM measurements. Joachim Koll, Silvio Neumann are thanked for their technical support and Dr. Mauricio Schieda for the help in UV experiments. Dr. Claudio Pistidda and Antonio Santoru are kindly acknowledged for the XRD measurements.

References

[1] T. Fukui, K. Murata, S. Ohara, H. Abe, M. Naito, K. Nogi, J. Power Sources 125 (2004) 17-21.
[2] G. Caravaggio, L. Nossova, R. Burich, Emiss. Control Sci. Technol. 2 (2016) 10-19.
[3] J. Muzart, Tetrahedron 59 (2003) 5789-5816.
[4] Y. Li, Z. Wu, S. Ye, New J. Chem. 39 (2015) 8108-8113.
[5] Y. Li, X.M. Hong, D.M. Collard, M.A. El-Sayed, Org. Lett. 2 (2000) 2385-2388.
[6] L. Yin, J. Liebscher, Chem. Rev. 107 (2007) 133-173.
[7] M. Oberholzer, C.M. Frech, Green Chem. 15 (2013) 1678-1686.
[8] Y. Niu, L.K. Yeung, R.M. Crooks, J. Am. Chem. Soc. 123 (2001) 6840-6846.
[9] M.M. Demir, M.A. Gulgun, Y.Z. Menceloglu, B. Erman, S.S. Abramchuk, E.E. Makhaeva, A.R. Khokhlov, V.G. Matveeva, M.G. Sulman, Macromolecules 37 (2004) 1787-1792.
[10] S. Agarwal, J.H. Wendorff, A. Greiner, Polymer 49 (2008) 5603-5621.
[11] D.H. Reneker, I. Chun, Nanotechnology 7 (1996) 216.
[12] G. Taylor, Proc. Royal Soc. A, The Royal Society, 1964, pp. 383-397.
[13] G. Taylor, Proc. Royal Soc. A, The Royal Society, 1969, pp. 453-475.
[14] S.V. Fridrikh, H.Y. Jian, M.P. Brenner, G.C. Rutledge, Phys. Rev. Lett. 90 (2003) 144502.
[15] T. Dai, N. Miletić, K. Loos, M. Elbahri, V. Abetz, Macro. Chem. Phys. 212 (2011) 319-327.
[16] M. Minnermann, H. Grossmann, S. Pokhrel, K. Thiel, H. Hagelin-Weaver, M. Bäumer, L. Mädler, Catal. Today 214 (2013) 90-99.
[17] K. Ebert, G. Bengtson, R. Just, M. Oehring, D. Fritsch, Appl. Catal. A Gen. 346 (2008) 72-78.
[18] N.B. McKeown, B. Gahnem, K.J. Msayib, P.M. Budd, C.E. Tattershall, K. Mahmood, S. Tan, D. Book, H.W. Langmi, A. Walton, Angew. Chem. Int. Ed. 118 (2006) 1836-1839.
[19] J.S. Bonso, G.D. Kalaw, J.P. Ferraris, J. Mater. Chem. A 2 (2014) 418-424.
[20] C. Zhang, P. Li, B. Cao, Ind. Eng. Chem. Res. 54 (2015) 8772-8781.
[21] C. Zhang, P. Li, B. Cao, J. Appl. Polym. Sci. 133 (2016).
[22] X. Chen, D. Zhao, Y. An, Y. Zhang, J. Cheng, B. Wang, L. Shi, J. Colloid Interface Sci. 322 (2008) 414-420.
[23] R. Hilke, N. Pradeep, P. Madhavan, U. Vainio, A.R. Behzad, R. Sougrat, S.P. Nunes, K.-V. Peinemann, ACS Appl. Mater. Interfaces 5 (2013) 7001-7006.
[24] A. Tena, R. Vazquez-Guilló, A. Marcos-Fernández, A. Hernández, R. Mallavia, RSC Adv. 5 (2015) 41497-41505.
[25] M.M. Khan, V. Filiz, G. Bengtson, S. Shishatskiy, M. Rahman, V. Abetz, Nanoscale Res. Lett. 7 (2012) 1-12.

[26] M.M. Khan, G. Bengtson, S. Shishatskiy, B.N. Gacal, M.M. Rahman, S. Neumann, V. Filiz, V. Abetz, Eur. Polym. J. 49 (2013) 4157-4166.
[27] M.M. Khan, V. Filiz, G. Bengtson, S. Shishatskiy, M.M. Rahman, J. Lillepaerg, V. Abetz, J. Membr. Sci. 436 (2013) 109-120.
[28] M.M. Khan, G. Bengtson, S. Neumann, M.M. Rahman, V. Abetz, V. Filiz, RSC Adv. 4 (2014) 32148-32160.
[29] K. Halder, M.M. Khan, J. Grünauer, S. Shishatskiy, C. Abetz, V. Filiz, V. Abetz, J. Membr. Sci. (2017).
[30] W.A. Feld, B. Ramalingam, F.W. Harris, J. Polym. Sci. A (1983) 319-328.
[31] L. Wannatong, A. Sirivat, P. Supaphol, Polym. Int. 53 (2004) 1851-1859.
[32] J.M. Deitzel, J. Kleinmeyer, D. Harris, N.B. Tan, Polymer 42 (2001) 261-272.
[33] W. Ogieglo, B. Ghanem, X. Ma, I. Pinnau, M. Wessling, J. Phys. Chem. B 120 (2016) 10403-10410.
[34] P.M. Budd, E.S. Elabas, B.S. Ghanem, S. Makhseed, N.B. McKeown, K.J. Msayib, C.E. Tattershall, D. Wang, Adv. Mater. 16 (2004) 456-459.
[35] M.J. Vaidya, S.M. Kulkarni, R.V. Chaudhari, Org. Process Res. Dev. 7 (2003) 202-208.
[36] M. Minelli, G. Cocchi, L. Ansaloni, M.G. Baschetti, M. De Angelis, F. Doghieri, Ind. Eng. Chem. Res. 52 (2013) 8936-8945.